

MIT Open Access Articles

*Stress concentration around an
atelectatic region: A finite element model*

The MIT Faculty has made this article openly available. **Please share** how this access benefits you. Your story matters.

Citation: Makiyama, A.M., L.J. Gibson, R.S. Harris, and J.G. Venegas. "Stress Concentration Around an Atelectatic Region: A Finite Element Model." *Respiratory Physiology & Neurobiology* 201 (September 2014): 101–110.

As Published: <http://dx.doi.org/10.1016/j.resp.2014.06.017>

Publisher: Elsevier

Persistent URL: <http://hdl.handle.net/1721.1/101909>

Version: Author's final manuscript: final author's manuscript post peer review, without publisher's formatting or copy editing

Terms of use: Creative Commons Attribution-NonCommercial-NoDerivs License



STRESS CONCENTRATION AROUND AN ATELECTATIC REGION: A FINITE ELEMENT MODEL

AM Makiyama¹, LJ Gibson¹, RS Harris², and JG Venegas³

¹Department of Materials Science and Engineering
Massachusetts Institute of Technology
Cambridge MA 02139

²Department_of Medicine
Pulmonary and Critical Care Unit
Massachusetts General Hospital
Harvard Medical School
Boston, MA 02114

³Department of Anesthesia
Massachusetts General Hospital
Harvard Medical School
Boston, MA 02114
(617) 726 8832
jvenegas@partners.org

Abstract

Lung parenchyma surrounding an atelectatic region is thought to be subjected to increased stress compared with the rest of the lung. Using 37 hexagonal cells made of linear springs, Mead et al. (J Appl Physiol 28 : 596-608, 1970) measured a stress concentration greater than 30% in the springs surrounding a stiffer central cell. We re-examine the problem using a 2D finite element model of 500 cells made of thin filaments with a non-linear stress-strain relationship. We study the consequences of increasing the central stiff region from one to nine contiguous cells in regular hexagonal honeycombs and random Voronoi honeycombs. The honeycomb structures were uniformly expanded with strains of 15%, 30%, 45% and 55% above their resting, non-deformed geometry. The curve of biaxial stress vs. fractional area change has a similar shape to that of the pressure-volume curve of the lung, showing an initial regime with relatively flat slope and a final regime with decreasing slope, tending towards an asymptote. Regular honeycombs had little variability in the maximum stress in radially oriented filaments adjacent to the central stiff region. In contrast, some filaments in random Voronoi honeycombs were subjected to stress concentration approximately 16 times the average stress concentration in the radially oriented filaments adjacent to the stiff region. These results may have implications in selecting the appropriate strategy for mechanical ventilation in ARDS and defining a "safe" level of alveolar pressure for ventilating atelectatic lungs.

STRESS CONCENTRATION AROUND AN ATELECTATIC

REGION: A FINITE ELEMENT MODEL

AM Makiyama¹, LJ Gibson¹, RS Harris² and JG Venegas³

Keywords: atelectasis, lung parenchyma, lung heterogeneity, finite element, cellular materials

Abbreviated title for running head: Stress concentration around an atelectatic region

Mailing address:

Antonio M Makiyama
Av. Paulista 352 cj 32
São Paulo SP Brazil
CEP 01310-000

Telephone: 55-11-3263 0186
55-11-98228 3261

e-mail: makiyama@alum.mit.edu

1-Introduction

Atelectasis, or alveolar collapse, causes a reduction of lung functional residual capacity and is a common clinical condition that occurs during general anesthesia for surgery (Brismar et al., 1985) and in disease states such as the acute respiratory distress syndrome (ARDS) (Gattinoni et al., 1986a, 1986b; Pelosi et al., 1994). ARDS is a syndrome characterized by localized regions of air-less lung tissue adjacent to expanding lung units (Gattinoni et al. 1986a, 1986b; Pelosi et al., 1994). Ironically, the mainstay of treatment for ARDS, namely positive pressure ventilation via a mechanical ventilator, has been found to cause or exacerbate lung injury. Although the exact mechanism for the injury still remains speculative, it has been hypothesized that high inflation pressures causing alveolar overdistension (Webb et al., 1974) and low end-expiratory pressures allowing airway closure, alveolar collapse and cyclic re-opening (Muscedere et al., 1994) may be the cause of what is termed ventilator-associated lung injury (VALI). Airway closure and alveolar collapse are also thought to potentiate VALI by reducing the number of alveoli available to distribute the tidal volume, thus increasing the likelihood of alveolar overdistension. Additionally, it has been postulated that atelectasis may cause stress concentrations in the tissues near the interface between the region of collapsed or non-

inflating alveoli and the surrounding ventiled alveoli (Denny and Schroter, 2006; Mead et al, 1970).

2-Previous Work

The stress concentration around a non-inflating region was first estimated by Mead (Mead et al., 1970) using a mechanical model consisting of a two-dimensional hexagonal array of coil springs, which was subjected to uniform tension at its outer boundary. They found the stress in the spring elements increased by about 50% with complete collapse of a central cell, giving rise to a condition of stress concentration in those members. Afterwards they compared predictions of stresses during lung expansion based on the mathematical model to changes seen with goat lung lobule inflation with a glued pleural disk and concluded that the mathematical model underestimated the stress (Takishima and Mead, 1972). Other investigators (Menkes et al. 1972a, 1972b) have found similar underestimation of stress concentration in the mathematical model and more sophisticated models of lung micro-mechanics have been published (Fung, 1988; , Kimmel et al. , 1987; Wilson and Bachofen, 1982). However, these models or continuum mechanics analyses give only estimates of average behavior and none have quantitatively examined the concentration of stress around a region of atelectasis in heterogeneous structures.

The aim of this research is to re-examine Mead's estimate of stress concentration around a non-inflating region of the lung using finite element analysis, with an asymmetric structure more like that of the lung. We model inflation of the lung around an existing atelectatic region, which does not inflate, while the rest of the lung around it does. The stresses within the atelectasis are not supported by the alveolar walls, but by a reduction in pressure of the intra-alveolar fluid, which, depending on surface tension and viscous forces, may not change in volume as the lung is dynamically inflated in mechanical ventilation. When the collapsed region expands little, it may be approximated as being rigid relative to the surrounding tissue.

In this paper we provide quantitative information on the stress concentration of stress bearing tissue elements in the parenchyma around such a region. We compare concentrations seen in a homogeneous hexagonal structure, similar to that of Mead's model, with those taking place in random structures, closer to the structure of the lung. We also analyze the impact of using linear and non-linear tissue elasticity in the calculations. The model is not intended to explain the process of atelectasis formation, parenchymal instability or its associated phenomena. However, our analysis is unique in that it demonstrates that individual stress bearing elements within a random

structure can be exposed to much higher stresses than the average stress around a non-expanding region and may also be much greater than those estimated for a uniform structure.

3-Cellular Materials Modeling

Many materials, both natural and synthetic, have a cellular structure made up of an interconnected network of filaments, struts or plates. Natural cellular materials include cork, wood and trabecular bone, as well as lung alveoli, of interest here. Engineering cellular materials include structural honeycombs and foams. The mechanical behavior of both two-dimensional, honeycomb-like materials with prismatic cells and three-dimensional, foam-like materials with polyhedral cells has been successfully described by modeling their mechanisms of deformation and failure (Gibson and Ashby, 1997). Random Voronoi cellular structures are typically used to model materials made of heterogeneously shaped cells. Although 2D models do not give identical results as 3D models Ma, Breen and Bates (Ma et al., 2013) utilized 2D non-linear springs to provide insights about network behavior a hexagonal-like array of the lung parenchyma, Ito (Ito et al, 2006) used a similar 2D network of hexagonal arrays and analyzed how the distribution of forces changes and the maximum force increases by adding non-linearity. Suki and Bates (Suki and

Bates, 2008) used a 2D Voronoi-like array of non-linear springs to model the lung parenchyma. They applied both springs running along the elements between the nodes and rotational springs at the nodes between adjacent cells. For the mechanical behavior of the lung tissue they considered a stress–strain curve with exponential stiffening. Here, we model two-dimensional cellular structures made of hexagonal and Voronoi cells, using an approach similar to Ma, Breen and Bates (Ma et al., 2013), Ito et al. (Ito et al, 2006) and Suki and Bates (Suki and Bates, 2008) respectively, where the filaments also represent the stress bearing elements in the parenchyma.

3.1 Generation of Voronoi and hexagonal models

Voronoi structures were initially developed to represent crystallization from a set of random nucleation points from which all the crystals begin to grow at the same time and continue to grow at the same rate. Two-dimensional Voronoi structures are created by drawing the perpendicular bisectors of lines connecting seed points generated with a uniform random distribution, as illustrated in **Fig. 1**. The Voronoi cell corresponding to an individual seed point is formed by the polygon of perpendicular bisectors that are closer to that seed point than to any other. In this study, we used hexagonal arrays and Voronoi honeycombs with approximately 500 cells within a square with

sides of approximately 22 cells. Voronoi honeycombs were generated using software developed by Silva and co-workers (Silva and Gibson, 1997; Silva et al. 1995). To produce cells with approximately uniform size, nucleation points closer than a critical distance, equal to 0.7 of the average edge length, were eliminated.

For both the hexagonal and Voronoi honeycombs the value of the filament thickness was set to give a constant thickness, normalized by the unit length, equal to 0.01. It is worth noting that the filament thickness is only used for the purpose of calculating the stress in the filament. For a 2D honeycomb, each filament is a two-dimensional object, with a length and a thickness. Given the normalization of the results by the stress in the filament for a honeycomb without atelectasis, the actual thickness of the filament becomes unimportant. Indeed, it is the relative differences in stress and not the actual value of stress within each filament that is relevant. To approximate the geometry of the stress bearing filaments in the lungs, we made the filaments slim by setting filament thickness to unit length ratio constant and equal to 0.01. In our case, for two dimensional filaments, one can think of the stress as the axial tensile force in each member divided by the product of the filament thickness times a unit depth out of the plane of the honeycomb. Non-expanding regions were defined by assigning exaggerated high stiffness to the filaments within a small

central region of the honeycomb. The high stiffness of the central region prevents it from deforming, simulating the lack of inflation of an atelectatic region that does not re-expand with lung inflation. These regions consisted of either a single central cell or that cell plus all its contiguous neighbors (**Fig. 2a, b**). Thus the diameter of these atelectatic regions was about $1/22$ or $1/7$ the size of the modeled square structure. Twelve Voronoi honeycombs were generated and analyzed, each from a different set of random seed points to quantify how the results varied among different Voronoi honeycombs. The results were averaged as described in the section *3.5 Stress Normalization* of this article.

3.2 Tissue elasticity

The stress-strain curve of the cell wall tissue was first modeled as linear elastic. The Young's modulus of the filaments representing the cell walls in the central stiff region was assumed to be 1000 times that of the surrounding filaments, which in practice essentially makes them rigid relative to the surrounding filaments.

In the lung, stress bearing elements are mostly made of collagen and elastin filaments, a combination that becomes stiffer as the less elastic collagen filaments straighten at high strains. In other words, at lower strains most of the stress in the tissue is borne by filaments of

elastin that are reasonably compliant, but as strain increases the collagen filaments that are initially soft start to straighten and assume the load-bearing role. Thus, in a second model, cell walls were represented by non-linear elastic filaments, with a strain-dependent Young's modulus as given by (West, 1977):

$$E = \frac{0.8E_0}{0.8 - \varepsilon} \quad (1)$$

Where E is the Young's modulus at a given strain, E_0 is the Young's modulus at zero strain and ε is the strain of the honeycomb wall (defined as the increase in length over the initial relaxed length). We note that eq (1) gives similar results for the dependence of modulus on strain as the constitutive equation proposed by Denny and Schroter (Denny and Schroter, 1997). Note that E approaches infinity when ε approaches 0.8; the model becomes invalid for strains equal to or greater than 0.8. Also a strain of 0.5 results in an increase of 125% in area of the two-dimensional structure and in an increase of 237.5% in volume for a three-dimensional structure.

3.3 Finite element analysis

Finite element analysis has been widely used to calculate the properties of materials with a cellular structure such as engineering honeycombs and foams. For instance, the elastic moduli and strength of random Voronoi honeycombs and of periodic closed-cell foams with

tetrakaidecahedral cells have been calculated in this way (Silva and Gibson, 1997; Silva et al., 1995; Simone and Gibson, 1998). Finite element analysis is especially well suited to study the effect of local inhomogeneities in the cellular structure on the mechanical response (Chen et al., 1999; 2001; Guo et al. 1994, 1999; Silva and Gibson, 1997). Here, the commercial finite element software ABAQUS (Hibbit Kartlsson & Sorensen, Inc. Pawtucket, RI.), was used to analyze the stresses in each member of the hexagonal and Voronoi honeycombs.

The outer shape of the structure analyzed was a square with length equivalent to that of approximately 22 contiguous cells. At the outer boundary of this square, we imposed equal biaxial displacements with incremental uniform displacements corresponding to engineering strains of 15, 30, 45 and 55%, where the engineering strain is expressed as the ratio of total deformation to the initial dimension of the material body in which the forces are being applied.

Equal biaxial displacement is considered the two-dimensional equivalent of volumetric expansion of three-dimensional polyhedral cells (e.g. pentagonal dodecahedra or tetrakaidecahedra) that have previously been used to model the lung (e.g. Denny and Schroter, 1997; Kimmel et al. , 1987). Our two-dimensional model is a representation of both the mode of deformation of the filaments (axial

deformation) as well as the stress-strain behavior of the filament material (equation 1).

To solve for local filament stress we made the following simplifying assumptions:

- The lung tissue network was represented by beam elements in a plane.
- The bending moments were negligible throughout the structure.
- The geometry of the outer boundary remained similar under the applied displacements; that is, its shape remained square.
- Non-linear geometric large deformations were assumed during the simulations.

We used three node quadratic beam elements type B22 from ABAQUS Finite Element Analysis software. In order to reduce the computational time in the cases with non-linear elasticity, field variables were created to allocate the desired initial Young's modulus to each member of the structure and to track changes in the Young's modulus in each filament as the applied strain increased. In the first increment of applied strain, the modulus of each filament was assigned the appropriate initial Young's modulus. For all increments after the first increment of strain, the internal strain in each member varied. For the second and subsequent strain increments, the Young's modulus in each filament

was recalculated using equation (1). The process was iterated until the desired final displacement was reached for the whole structure. Finite Element Analysis requires that the equations of equilibrium are satisfied, so that there is a force balance at each node, it is standard practice to apply either forces or displacements to the nodes of the structure in an incremental manner up to the desired maximum force or displacement. In our case, we chose to apply incremental displacements to the boundary of the model.

3.4 Cell wall grouping and orientation

The stress concentration on individual elements depended not only on their distance to the atelectatic region, but also on the relative orientation of them. For that reason, filaments were grouped as a function of their orientation and their distance, r , from the center of the honeycomb. Three different orientations (radial, intermediate and tangential) were defined based on the magnitude of the angle θ between the filament orientation and the radial vector from the center of the model to the center of that member: filaments with $0^\circ < \theta < 30^\circ$ were defined to be in the radial orientation; those with $30^\circ < \theta < 60^\circ$ were defined to be intermediate orientation and those with $60^\circ < \theta < 90^\circ$ were defined to be in the tangential orientation.

Nine different radial locations were defined by concentric rings around the central stiff region, equally radially spaced in increments of two average filament lengths. The average filament length is the sum of all individual filament lengths divided by the total number of filament in the structure.

3.5 Stress Normalization

Stress Normalization is a standard procedure in calculating stress concentration (for example, around a stiff inclusion or a hole) to compare the stresses in the structure with the stiff inclusion or the hole to those in the uniform structure, without the stiff inclusion or the hole.

For each level of global strain, the effect of a stiff atelectatic region on local stress distribution of surrounding filaments was characterized by normalizing the stress in each filament by that measured in the same structure at the same strain but with the central filaments having values of Young's modulus equal to the rest of the structure. In other words, stress was normalized to that of each filament during equivalent expansion of the system without the central atelectasis. The effect of a non-expanding (and thus stiff) central atelectatic region on the local stress distribution of surrounding elements was thus characterized by the relative increase in force in each element compared with that estimated for the same structure but

with an expanding central region. This normalized stress gave an index of the stress concentration caused by the central stiff region.

For each condition and model studied, the normalized stress on the Voronoi honeycomb filaments, binned by orientation (radial, intermediate and tangential) and radial distance (r) from the atelectatic region, were characterized by the following three measures: their average, their individual maximum (ind max), and the average of the maximum for the 12 Voronoi honeycombs (avg max), and the respective standard deviations (Table 2).

4 Results

For the regular hexagonal honeycomb with non-linear cell wall elasticity (and no central stiff region), the two-dimensional equivalent of the pressure-volume curve is the stress-area curve shown in **Fig. 3**. The equivalent continuum stress applied at the boundary, σ , is the total normal force at a boundary (calculated from the normal component of force in each member along one side of the boundary, divided by the current cross-sectional area of the boundary). We assume that the structure has unit depth in the third dimension. The structure is in equilibrium, so that the component of the expansion force normal to one face of the structure is equal and opposite to that on the opposite face. This equivalent stress is then normalized with

respect to the initial (unstressed) Young's modulus of the cell filaments, E_0 . The shape of the curve is qualitatively similar to that of the lung pressure-volume curve, showing a regime of relatively constant slope at low strains, and a regime of decreasing slope approaching an asymptote at high strains. We note that the filament modulus goes to infinity at a member strain of 0.8 (eqn 1), limiting the change in area of the honeycomb relative to the initial area to values less than 2.24 because the applied stress approaches infinity.

The two-dimensional bulk modulus of the regular honeycomb can be calculated from:

$$K_{2D} = \frac{d\sigma}{\frac{dA}{A_0}} = \frac{A_0}{\frac{dA}{d\sigma}} \quad (2)$$

Fitting a second order polynomial to the $\Delta A/A_0$ versus σ/E_0 curve of

Fig. 3, we obtain the following equation:

$$\frac{\Delta A}{A_0} = \alpha \left(\frac{\sigma}{E_0} \right) + \beta \left(\frac{\sigma}{E_0} \right)^2 \quad (3)$$

Where:

$$\alpha = 8.33 \times 10^3$$

$$\beta = -7.57 \times 10^6$$

The Equation (3) was obtained from the results of non-linear finite element analysis simulations involving large deformations and non-

linear variation of the Young's modulus with strain given by equation (1).

Taking the derivative $dA/d\sigma$ and substituting into eq (2) we obtain:

$$\frac{K_{2D}}{E_0} = \frac{1}{\gamma + \delta \left(\frac{\sigma}{E_0} \right)} \quad (4)$$

Where:

$$\gamma = 8.33 \times 10^3$$

$$\delta = -1.51 \times 10^7$$

For the regular hexagonal honeycomb with the linear elastic cell wall (and no inclusion), the values of the coefficients of the eq. (3) were found to be $\alpha=0$ and $\beta=6.4 \times 10^7$. This equation represents an approximation of the finite element results for the change in area, $\Delta A/A_0$, as a function of normalized stress. For values of equivalent stress associated with the maximum strains imposed, ($\sigma/E_0 < 0.0002$), the relative increase in area scales with the square of the stress, a non-realistic condition for the lung. For the results of the non-linear elastic filaments in equation (3), however, the coefficient β of the quadratic term is negative and the slope of the curve decreases as the values of σ/E_0 increase, resulting in a global stiffening of the system with inflation that resembles the pressure-volume relationship for lung.

The linear elastic cell wall models, which simulate the mechanical behavior of the hexagonal models of previous related research (Mead et al., 1970; Wilson, 1972) do not give physiologically plausible results since their approximation by equations (3), with $\alpha=0$, has a parabolic shape with a positive coefficient β , and scales with the square of the stress imposed. As a consequence, the slopes of these curves increase with σ/E_0 resulting in unstable behavior.

Applied equal biaxial tensile strain induces axial loads in each member of a regular hexagonal honeycomb so that each cell remains a regular hexagon with all struts equally lengthened. The presence of a central stiff region distorts the hexagonal shape of the cells adjacent to the inclusion, causing a stress concentration (**Fig. 2a, b right**). As the size of the inclusion is made greater, the radial distance over which the hexagonal shape is distorted increases. For both sizes of the local stiff region studied here, the cell deformation reverts to the regular hexagonal pattern well within the boundary of the model, indicating that edge effects are small.

The decay of the average normalized stress in the radial members of the regular hexagonal honeycomb, is plotted in **Fig. 4**. For the regular hexagonal honeycombs, the radially oriented members immediately adjacent to the stiff region are subjected to nearly identical stress and have the highest strain and stress concentration.

The equivalent continuum solution for the radial stress concentration around a rigid cylindrical inclusion in a linear elastic medium under equal biaxial tension is also plotted (Goodier, 1933). The stress concentration in the radial members immediately adjacent to the stiff region increased with both the applied strain and the size of the stiff region and was generally higher for the non-linear elastic filament modulus (eq 1) than for the linear elastic model with constant filament modulus (**Table 1, Fig. 5**).

To achieve the same strain in the honeycomb with the stiff region, the stress remote from the stiff region is slightly higher than that in the honeycomb with spatially uniform values of Young's modulus. As a result, the average normalized stress plotted in **Fig. 4** decays to a value slightly higher than unity.

For the Voronoi honeycombs with non-linear cell wall elasticity (and no local stiff region), the change in area as a function of stress is shown in **Fig. 3**, where the curve that represents the Voronoi honeycombs was plotted from a representative sample of Voronoi arrays. The overall shape of the curve is again similar to that of the regular hexagonal honeycomb as well as that of the dog lung pressure-volume curve (Lai-Fook et al., 1976), and the bulk modulus can be calculated from it in the same way. In this case, we found the

coefficients of eq. (3) as $\alpha=8.3 \times 10^3$ and $\beta=-8.00 \times 10^6$ and the coefficients of eq. (4) as $\gamma=8.3 \times 10^3$ and $\delta=-1.6 \times 10^7$.

Eq (3) gives stress-area curves that are similar to measured pressure-volume curves in the lung (Mead et al., 1970) and eq. (4) gives a dependence for the bulk modulus on stress similar to that measured in the dog lung (Lai-Fook et al., 1976) and these two equations provide a similar set of curve shapes either for the regular hexagonal honeycomb or for the random Voronoi honeycomb.

For the Voronoi honeycomb with the linear elastic cell wall (and no local stiff region), the finite element results for the change in area, $\Delta A/A_0$, as a function of normalized equivalent stress, σ/E_0 , can be approximated by Eq. (3) with coefficients $\alpha=0$ and $\beta=2.7 \times 10^8$. Similar to the case of the regular hexagonal honeycomb, for values of normalized equivalent stress, σ/E_0 , associated with the maximum strains imposed in this simulation, there is a quadratic increase in area with increasing stress, resulting, as mentioned previously, in an unstable behavior. In contrast, the results for the non-linear elastic filaments, and also the pressure-volume relationship for lung, the curves reach a plateau value.

As for the regular honeycomb model, the local stiff region in the Voronoi honeycomb gives rise to a stress concentration, which, on average, is larger in the radially oriented members in given "band" (at

a particular radial distance from the center of the model) compared with members in either the tangential or intermediate orientations. Due to the heterogeneity of the structure, there is a distribution of stresses in the radial members adjacent to the stiff region. In **Table 2**, we report three normalized stresses:

- the average normalized stress in the radial members in the cells adjacent to the stiff region for all 12 Voronoi honeycombs
- the average, over all 12 Voronoi honeycombs, of the maximum normalized stress in the radial members adjacent to the stiff region in each Voronoi honeycomb
- the individual maximum normalized filament stress of all the filaments in all 12 Voronoi honeycombs (this was always a filament in the radial orientation but is not always adjacent to the stiff region)

The average normalized stress in the radial members adjacent to the stiff region increases slightly with strain and with the size of the stiff region; the increases are more pronounced for the non-linear elastic filaments than the linear elastic filaments, as might be expected. The variability between the average stress values of the 12 Voronoi honeycombs was analyzed and the standard deviation of the normalized stresses in any orientation, at any radial distance among the 12 Voronoi honeycombs was in the range of 0.024 to 0.045.

The decay in the average normalized stresses in the radially oriented members in the Voronoi honeycombs are plotted in **Fig. 6**, along with the equivalent continuum solution for a rigid cylindrical inclusion in a linear elastic medium under equal biaxial tension: The finite element analysis of the discrete Voronoi honeycomb is again similar to the continuum analysis. The Voronoi honeycombs with the single cell stiff region are less well represented by the continuum analysis than those for the multiple cell stiff region, as might be expected. For the non-linear elastic case with 55% applied strain, we were not able to obtain a solution due to lack of convergence in the iterative solution.

5 Discussion

The consequences of non-expanding lung parenchyma in atelectasis can range from a temporary alteration in lung function to serious lung tissue damage. At the simplest level, atelectasis can result in hypoxemia when unoxygenated blood flows through the capillaries of unaerated alveoli. More recently, a more dangerous consequence of atelectasis has been theorized to occur during ARDS (Dreyfuss and Saumon, 1998). Based on the original work of Mead (Mead et al., 1970), it has been postulated that the heterogeneity in lung expansion during ARDS may result in a concentration of stress in

tissues around the atelectatic regions causing injury at otherwise acceptable levels of distending pressures.

Using a network of springs similar to Mead, Wilson (Wilson, 1972) developed a continuum mechanics analysis of a two-dimensional mechanical model of lung parenchyma and described the analysis of deformation of an elastic tube embedded in an elastic continuum made up of a hexagonal array of linear springs. Applying the finite element method, we solved the continuum mechanics deformation problem of hexagonal array of linear springs described in his work. The values of additional tension applied to the inner springs in his paper, which corresponds to our values of stress concentration, were found to be quantitatively consistent with Wilson's results.

Different approaches have been used to model geometrically complex, three-dimensional, foam-like structures such as: *structural analysis* of polyhedral unit cell models, *dimensional analysis* of cells that deform and fail by the same mechanisms as foams, *finite element analysis* of random Voronoi and non-Voronoi structures, and continuum approximations of those structures. Unit cell models have been used to analyze the response of idealized polyhedral cells to mechanical loading (Ko, 1965, Takishima et al., 1972; Wilson and Bachofen, 1982). Unit cell models of lung parenchyma have been proposed by Kimmel and co-workers (Kimmel and Budiansky, 1990;

Kimmel et al., 1987), who analyzed a pentagonal dodecahedral cell, and by Denny and Schroter (Denny and Schroter, 1995, 1997, 2000, 2006), who analyzed tetrakaidecahedral cells, and more recently by L. Wiechert and Wall, who used micro scale multi-physics approach to analyze tetrakaidecahedral cells (Wiechert and Wall, 2010). Here we present an analysis of random Voronoi structure that is likely to represent more accurately the human lung in both the healthy and injured states, and compare it with results from hexagonal honeycombs and continuum approximations.

In the hexagonal honeycomb with the linear elastic filaments, the decay in the stress concentration with radial distance away from the inclusion is similar to that for the continuum analysis of a rigid cylindrical inclusion in a linear elastic medium under equal biaxial tension (**Fig. 4a, b**). However, in the honeycomb model, the stress concentration depends on the applied strain and the size of the local stiff region, unlike the continuum solution. In the honeycomb with a local stiff region of a given size, the members close to the stiff region realign towards the radial direction to accommodate the difference in stiffness between the stiff region and the bulk of the honeycomb, with the degree of realignment increasing with the applied strain. The changing structure of the honeycomb gives rise to the strain dependence of the stress concentration. Similarly, for a given strain,

as the size of the local stiff region increases, the distortion of the regular hexagonal network increases, so that again, the changing structure of the honeycomb produces a dependence of the stress concentration on the size of the local stiff region. We note that as the size of the stiff region increases in the linear elastic regular hexagonal honeycomb, the strain dependence decreases, and the stress concentration is closer to the continuum solution. In the limit of a local stiff region with higher number cells (with roughly 10 cells across its diameter) and a sufficiently large model (with roughly 10 inclusion diameters, or 100 cells, in the radial direction), we expect the honeycomb result to approach the continuum solution.

For the honeycomb with the larger stiff region, the stress concentration at the outer boundary of the model is affected by strain more than in the other cases. As mentioned previously, the size of these non-expanding regions are respectively (for one cell and for a set of 6 to 9 contiguous cells) about $1/22$ and $1/7$ the size of the square structure (**Fig. 2a, b left**) or the circle inscribed within it. The corresponding approximate ratios of the non-expanding area over the rest of the model containing normally expanding cells, A_r , are 0.002 and 0.018. In the case of 6 to 9 contiguous stiffened cells the non-expanding area is about 9 times larger than the area of the one rigid cell structure. This means that for the same total increase in the area

of the system, the reduced deformation of the larger stiffened area would have the effect of reducing the number of expanding hexagons and increasing the stress throughout the system, including those at the boundary of the square structure.

For the Voronoi honeycomb models, the maximum stress occurred in the radially oriented filaments adjacent to the stiff region. The average stress in these members was almost identical to those of the regular hexagonal honeycomb for both linear and non-linear elastic filaments. (**Table 1, Fig. 5**). For the reasons described above, the stress concentration increases with increasing strain (by about 15% for the linear filament and about 20% and 30% for the non-linear filament with 1 and 7 cells respectively) and with increasing size of the stiff region (by about 10% for the linear filament and about 12% for the non-linear filament).

In the Voronoi honeycomb models, the average stress in the radial members adjacent to the stiff region was slightly lower but generally within 6% of that of the regular hexagonal honeycomb, for the same configuration and strain (e.g. linear elastic filament, 1 stiff cell, 15% strain), suggesting that the *average* response of the random honeycomb is similar to that of the regular hexagonal honeycomb (**Tables 1, 2**). The *variation* in the filament stresses in the Voronoi honeycomb was much larger than that in the regular hexagonal

honeycomb, however. For instance, for the case of the non-linear elastic filament, with 6-9 cells in the stiff region, at 45% strain, the average, over all 12 Voronoi honeycombs, of the maximum radial stress concentration in the members adjacent to the stiff region was 2.43. The stresses in the Voronoi honeycomb were much more variable than in the regular honeycomb. The average maximum stress in the 12 simulations was 2.43, almost 3 times the stress concentration given by the regular honeycomb model (1.54), but it could reach a maximum of 16 times in a individual filament (9.59). For the Voronoi honeycombs, the decay in average stress concentration with radial distance away from the stiff region was similar to that for the regular hexagonal honeycombs. For the linear elastic Voronoi honeycomb, the dependence of the stress concentration on strain decreases with increasing size of the local stiff region, and the stress concentration approaches that of the linear elastic continuum solution as the size of the local stiff region increased (**Fig. 6 a,b**). For the non-linear Voronoi honeycomb, the average stress concentration adjacent to the local stiff region is smaller than that of the regular hexagonal honeycomb (**Fig. 6 c,d**).

We compared our finite element results with the continuum solution for the stress concentration around a rigid cylindrical inclusion in a linear elastic medium under equal biaxial displacement. As

mentioned previously, in our analysis, we model the inflation of the lung around an existing non-expanding region that was already collapsed and did not inflate as the rest of the lung inflated. The appropriate two-dimensional continuum comparison is that for the stress concentration around a rigid cylindrical inclusion in a linear elastic medium under equal biaxial displacement. The lung mechanics literature has often made use of the Lamé continuum solution for the stresses in a thick cylinder with a central hole under differing internal and external pressures. This solution is relevant to the mechanics of the interaction of the bronchi and pulmonary vessels and the lung parenchyma surrounding them (see, for instance, Lai-Fook (Lai-Fook, 1979; Lai-Fook et al. 1977) and the review by Kamm (Kamm, 1999)) and could be applied to modeling stress concentrations around a rigid region, as described in this study. If the external cylinder of Lamé's formulation is made very large, and the pressure within the hole is reduced to the point where the hole achieves the size of the rigid inclusion, Lamé's solution gives equivalent results to the continuum solution of Goodier (Goodier, 1933) used here.

We also note that continuum models also have their own limitations in describing the mechanics of random structures with discrete stress bearing elements: by their nature, they cannot describe the variability in the stresses in individual stress bearing

elements. One strength of the finite element analysis described in this study is the ability to obtain a quantitative description of the variability in the stresses in filaments at the same radial distance from the inclusion.

The maximum stress concentration around a rigid spherical inclusion in a linear elastic medium under external outward pressure (the equivalent three-dimensional continuum result) is 1.62 (**Fig. 7**). For the two-dimensional case, we found that the *average* stress concentration in the radial members adjacent to the stiff region in the Voronoi honeycomb was similar to both the *average* stress concentration in the radial members of the regular hexagonal honeycomb adjacent to the stiff region and to the stress concentration given by the 2D continuum analysis. Extrapolating our honeycomb results to three dimensions, we suggest that the *average* stress concentration in a three-dimensional random Voronoi structure will be very close to the continuum value of 62% and that the *average maximum* stress may reach approximately 3 times this value, but it may reach a maximum of 16 times in a individual filament. These are much higher stress concentrations than the value of 50% suggested by Mead.

Our study has a number of limitations. We analyzed two-dimensional, rather than three-dimensional structures. As discussed

above, we have suggested an extrapolation of the two-dimensional results to three-dimensions, using the continuum solutions and the variability we found in the random two-dimensional Voronoi structure. A three-dimensional Voronoi structure sufficiently large to eliminate edge effects would have roughly 100,000 filaments, which is computationally possible with HPC cluster computing. We hope that the two-dimensional model presented here serves to motivate a similar work in three-dimensions.

In the models presented here, we did not simulate the creation of atelectasis from an inflated state, but we expanded the lung models bi-axially from an initially unstressed state. The results of Finite Element Analysis simulations showed that, unlike the hexagonal honeycombs structures, a small number of tangential filaments of the Voronoi honeycomb structure were under slight compression due to the high anisotropy of the structure. However, that amount of compression was negligible compared with the tension of radial members. In addition, the choice of very slim filaments resulted in negligible bending moments on the filament joints. By expanding the lungs to the same volume as without the stiff region, we are assuming that lung volume does not change, which is unlikely to happen unless the area of atelectasis is small. A slight reduction in lung volume would tend to lessen the magnitude of the stress concentration.

A second limitation in our model was that we did not include the effect of surface tension on the stress concentrations. Surface tension effects are complex and depend on the microstructure of the alveolus and the thickness of the fluid layer. Typically surface tension should create a force that, for a given degree of lung expansion, would increase the required inflation pressure, or, for a given degree of inflation pressure would reduce the stress load on the stress bearing alveolar filaments. However the magnitude of this effect depends on the radius of curvature of the air-liquid interface at the alveolus. If the deformation of alveolar shape in regions near the atelectatic region elongates the alveolus in the radial direction away from the atelectasis, the radius of curvature of the air-liquid interface near the collapsing units would tend to be reduced. This would tend to increase the surface tension and make the system unstable promoting the growth of the atelectasis and thus increase the stress of radial filaments, further exaggerating the stress concentration on them. Furthermore, it has been suggested that, as an approximation, surface tension effects can be combined with tissue elasticity, so that the additional stiffness arising from area changes in the fluid layer may be incorporated into the non-linear tissue elasticity (Kimmel et al., 1987 ; Lanir, 1983). We note that our results for the normalized stress concentrations were dependent on the cell wall elasticity: we obtained

moderately higher stress concentrations results for non-linear elasticity in the solid cell wall material. This suggests that incorporation of surface tension effects could further exaggerate the magnitude of the stress concentration. It will be useful to substantiate these speculations in future modeling.

A further limitation of our model was that we assumed the walls of the honeycombs to be initially straight, with no externally applied stress and with no internal stress in the walls. In contrast, in the lung, the alveolar walls are straightened by slight pressurization of the lung. We suggest that our results may not have been substantially affected by this assumption for the degree of lung inflations studied given the normalization of the data, taking the stresses in the near field members relative to those in the far field at a particular level of global strain which was always positive.

6 Conclusion

The two-dimensional approximation of our model with non-linear elasticity gives a reasonable representation of the behavior experimentally measured in the lung in terms of the pressure-volume behavior as well as the dependence of bulk modulus on pressure. This is not the case for the models with linear elasticity. In the regular hexagonal model, the radially oriented filaments adjacent to the stiff

region undergo the highest stress concentration; as a result of the regularity of the hexagonal model, all of these members undergo identical stress. The stress decay in the radial members of the regular hexagonal honeycomb approximately follows the continuum analysis for a rigid cylindrical inclusion in a linear elastic medium. In the Voronoi honeycombs, the *average* stress concentration in the radially oriented members adjacent to the stiff region is very close to that in the regular hexagonal honeycomb (and in the continuum analysis). However, due to the inhomogeneity in the structure, there is a large variation in the stress concentration of individual members. As mentioned previously, the *average maximum* stress is almost 3 times the stress concentration given by the regular honeycomb, but in an individual member may reach approximately 16 times the average stress. The continuum analysis of a rigid sphere in a linear elastic continuum of Goodier (Goodier, 1933) gives the maximum stress concentration adjacent to the sphere as 1.62. Extrapolation of our two-dimensional results to a three-dimensional Voronoi structure suggests that the *average* stress concentration in the radially oriented members should be slightly higher than 1.62 and that the average maximum stress could be almost 3 times this value, but in individual members this magnitude could be could about 16 times. These are

considerably higher than Mead's estimate of a stress concentration of 50%.

In the lungs this would translate into the finding that in atelectatic regions, ventilation with pressures that could be considered safe in homogeneous lungs can result in substantially higher stresses, and injury, to parenchyma adjacent to the atelectasis. For example, ventilation with pressures limited to less than 30 cm H₂O could result in average local stress concentrations in individual stress bearing elements equivalent to a uniform stress of roughly 48 cm H₂O (1.62 x 30 cm H₂O) and much greater in some filaments considering the additional concentration caused by the non-uniformity of the alveolar walls. These results may have implications in selecting the appropriate strategy for mechanical ventilation in ARDS and defining a "safe" level of alveolar pressure for ventilating atelectatic lungs.

References

Andrews EW, Gioux G, Onck PR and Gibson LJ Size effects in ductile cellular solids Part II: Experimental Results. *Int. J. Mech. Sci.*,43:701-713, 2001.

Brismar B, Hedenstierna G, Lundquist H, Strandberg A, Svensson L and Tokics L. Pulmonary densities during anesthesia with muscular relaxation--a proposal of atelectasis. *Anesthesiology* 62: 422-428, 1985.

Chen C, Lu, TJ and Fleck, NA- Effect of imperfections on the yielding of two-dimensional Foams-*J Mech Phys Solids* 47 2235-72 -1999

Chen C, Lu, TJ and Fleck NA- Effect of inclusions and holes on the stiffness and strength of honeycombs- International Journal of Mechanical Sciences 43 pp 487-504 2001

Denny E and Schroter RC The mechanical behaviour of a mammalian lung alveolar duct model J. Biomech. Eng. 117: 254-261, 1995.

Denny E and Schroter RC Relationships between alveolar size and fibre distribution in a mammalian lung alveolar duct model. J. Biomech. Eng. 119: 289-297, 1997.

Denny E and Schroter RC Viscoelastic behavior of a lung alveolar duct model J. Biomech. Eng. 122: 143-151, 2000.

Denny E and Schroter RC - A model of non-uniform lung parenchyma distortion Journal of Biomechanics 39 652-663, 2006

Dreyfuss D and Saumon G. Ventilator-induced lung injury: lessons from experimental studies. Am J Respir Crit Care Med 157: 294-323, 1998.

Fung YC. A model of the lung structure and its validation. J Appl Physiol 64: 2132-2141, 1988.

Gattinoni L, Mascheroni D, Torresin A, Marcolin R, Fumagalli R, Vesconi S, Rossi GP, Rossi F, Baglioni S, Bassi F and et al. Morphological response to positive end expiratory pressure in acute respiratory failure. Computerized tomography study. Intensive Care Med 12: 137-142, 1986a.

Gattinoni L, Presenti A, Torresin A, Baglioni S, Rivolta M, Rossi F, Scarani F, Marcolin R and Cappelletti G. Adult respiratory distress syndrome profiles by computed tomography. J Thorac Imaging 1: 25-30, 1986b.

Gibson LJ and Ashby MF Cellular Solids: Structure and Properties. Second Edition. Cambridge University Press 1997.

Goodier JN, Concentration of Stress Around Spherical and Cylindrical Inclusions and Flaws, J. Appl. Mech, 55: 39-44, 1933.

Guo XE, McMahon TA, Keaveny TM, Hayes WC and Gibson LJ - Finite Element Modeling of Damage accumulation in Trabecular Bone under Cyclic Loading-J Biomechanics Vol 27 No 2, pp 145-155, 1994

Guo XE, and Gibson LJ- Behaviour of intact and damaged honeycombs: a finite element study- International Journal of Mechanical Sciences 41 pp 85-105 1999

Hibbit Kartlsson & Sorensen, Inc. Pawtucket, RI. - ABAQUS User's Manual. www.abaqus.com November 2013

Ito S, Bartolák-Suki E, Shipley JM, Parameswaran H, Majumdar A, and Suki B Early Emphysema in the Tight Skin and Pallid Mice Roles of Microfibril-Associated Glycoproteins, Collagen, and Mechanical Forces Am J Respir Cell Mol Biol Vol 34. pp 688-694, 2006

Kamm RD Airway wall mechanics. Ann. Rev. Biomed. Eng.1: 47-72, 1999.

Kimmel E and Budiansky B. Surface tension and the dodecahedron model for lung elasticity. J Biomech Eng 112: 160-167, 1990.

Kimmel E, Kamm RD and Shapiro AH. A cellular model of lung elasticity. J Biomech Eng 109: 126-131, 1987.

Ko WL Deformations of foamed elastomers. J. Cellular Plastics 1: 45-50, 1965.

Lai-Fook SJ A continuum mechanics analysis of pulmonary vascular interdependence in isolated dog lobes. J. Appl. Physiol.: Respirat. Environ. Exercise Physiol. 46: 419-429, 1979.

Lai-Fook SJ, Wilson TA, Hyatt RE and Rodarte JR Elastic constants of inflated lobes of dog lungs. J. Appl. Physiology 40: 508-513, 1976.

Lai-Fook SJ, Hyatt RE, Rodarte JR, and Wilson TA Behavior of artificially produced holes in lung parenchyma. J. Appl. Physiol.: Respirat. Environ. Exercise Physiol. 43: 648-655, 1977.

Lanir Y Constitutive equations for the lung tissue. J. Biomech Eng 105: 374-380, 1983.

Ma, B., Breen, B. and Bates, J.H.T. Influence of parenchymal heterogeneity on airway-parenchymal interdependence. *Respiratory Physiology & Neurobiology*. 2013 - In Press
<http://dx.doi.org/10.1016/j.resp.2013.06.005>

Mead J, Takishima T, and Leith D-Stress distribution in lungs: a model of pulmonary elasticity. *J Appl Physiol* 28 : 596-608, 1970

Menkes H, Gamsu G, Schroter R and Macklem PT. Interdependence of lung units in isolated dog lungs. *J Appl Physiol* 32: 675-680, 1972a.

Menkes H, Lindsay D, Wood L, Muir A and Macklem PT. Interdependence of lung units in intact dog lungs. *J Appl Physiol* 32: 681-686, 1972b.

Muscledere JG, Mullen JB, Gan K and Slutsky AS. Tidal ventilation at low airway pressures can augment lung injury. *Am J Resir Crit Care Med* 149: 1327-1334, 1994.

Onck PR, Andrews EW and Gibson LJ Size effects in ductile cellular solids Part I: Modelling. *Int. J. Mech. Sci.*, 43: 681-699, 2001.

Pelosi P, D'Andrea L, Vitale G, Pesenti A and Gattinoni L. Vertical gradient of regional lung inflation in adult respiratory distress syndrome. *Am J Respir Crit Care Med* 149: 8-13, 1994.

Silva M J and Gibson LJ- The effects of non-periodic microstructure and defects on the compressive strength of two-dimensional cellular solids- *Int J Mech. Sci.* 39, 549-563, 1997

Silva MJ, Hayes C, WC and Gibson LJ-The Effects of Non-Periodic Microstructure on the Elastic Properties of Two-Dimensional Cellular Solids- *Int. J. Mech. Sci.* Vol 37 No11, pp 1161-1177, 1995

Simone AE, and Gibson LJ- Effects of Solid Distribution on the Stiffness and Strength of Metallic Foams *Acta mater.* Vol 46 No6 pp 2139-2150 1998

Suki B, Bates JTH Extracellular matrix mechanics in lung parenchymal diseases *Respiratory Physiology & Neurobiology* 163, 33-43 2008

Takishima T and Mead J. Tests of a model of pulmonary elasticity. J Appl Physiol 33: 576-581, 1972.

Webb HH and Tierney DF. Experimental pulmonary edema due to intermittent positive pressure ventilation with high inflation pressures. Protection by positive end-expiratory pressure. Am Rev Respir Dis 110: 556-565, 1974.

West John B, Regional Differences in the Lung - Academic Press 1977 pp 281-322

Wiechert L and Wall WA- A nested dynamic multi-scale approach for 3D problems accounting for micro-scale multi-physics Comput. Methods Appl. Mech. Engrg. 199 1342–1351 2010

Wilson TA A continuum analysis of a two-dimensional mechanical model of the lung parenchyma. J. App Physiol 33: 472-478, 1972.

Wilson TA and Bachofen H. A model for mechanical structure of the alveolar duct. J Appl Physiol 52: 1064-1070, 1982.

Figure Captions

Figure 1 Construction of a two-dimensional Voronoi structure. The solid lines are the perpendicular bisectors. The dashed lines are the lines connecting the seed points.

Figure 2 Left Regular hexagonal honeycombs (top) and Voronoi honeycombs (bottom) showing the location and number of stiff central cells representing atelectatic regions (filled cells). Simulations were conducted in both architectures for a single central rigid cell (a) or for a central cell and the surrounding first layer of cells (b). **Right** - Typical deformations of the non-linear elastic filaments of the hexagonal (top) and Voronoi honeycombs (bottom) for one central rigid cell (a) and multiple central rigid cells (b). (Case for a biaxial strain of 55% with magnification factor of 2.5).

Figure 3 Plots of applied strain ($\Delta A/A_0$) against "true biaxial stress" (the sum of filament forces divided by the current area) normalized by the initial filament modulus of elasticity, E_0 , for non-linear elastic filaments defined by equation (1). Data obtained from simulations expanding the hexagonal (filled squares) and Voronoi (open squares) models (with no central stiff region). The shape of the plots resembles the pressure-volume relationship for the lung.

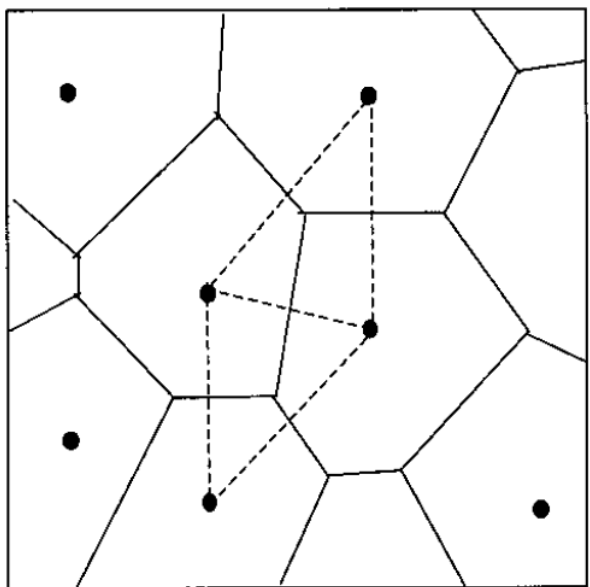
Figure 4 The average normalized stress in the radial members of the regular hexagonal honeycombs plotted against the radial distance (before deformation) from the center of the inclusion, normalized by the inclusion radius, r/a . (a) Linear elastic, 1 stiff cell (b) linear elastic, 7 stiff cells (c) non-linear elastic, 1 stiff cell (d) non-linear elastic, 7 stiff cells. The dashed line in each figure is the 2D solution for a rigid cylindrical inclusion in a linear elastic continuum. Strain=15% (◆), strain=30% (■), strain=45% (▲), strain=55% (×).

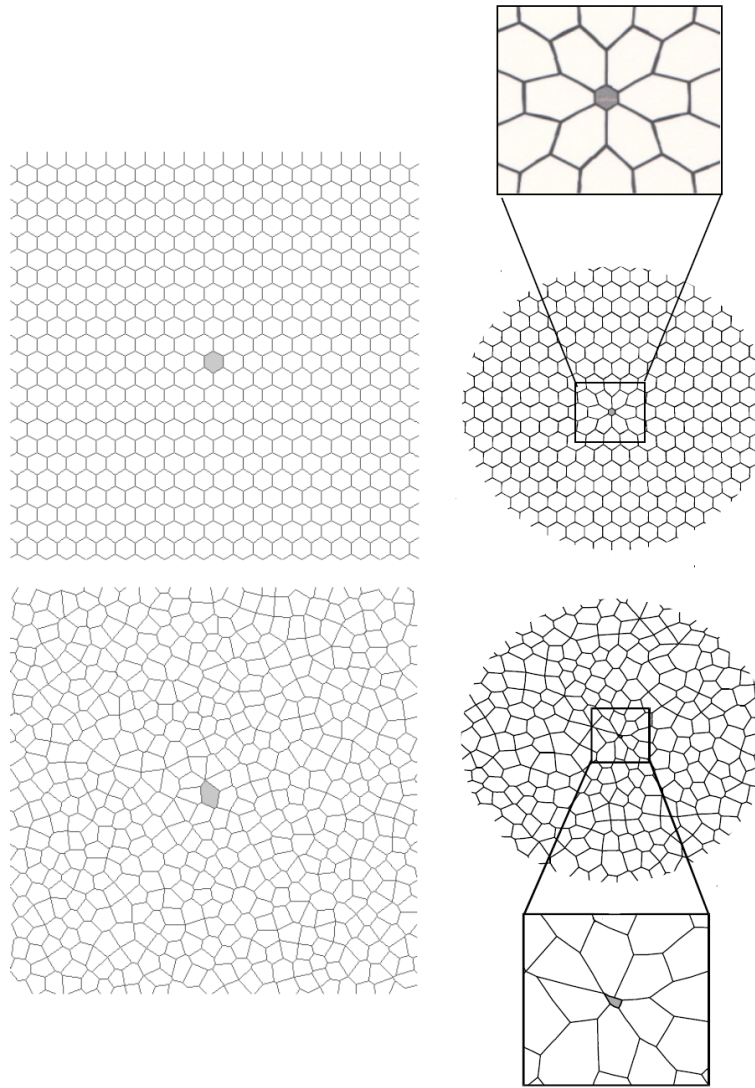
Figure 5 Normalized stress concentration in the radial members immediately adjacent to the stiff region for the regular hexagonal honeycombs.

Figure 6 The average normalized stress in all radially oriented members in all 12 Voronoi honeycombs plotted against distance from the center of the stiff region (a) Linear elastic

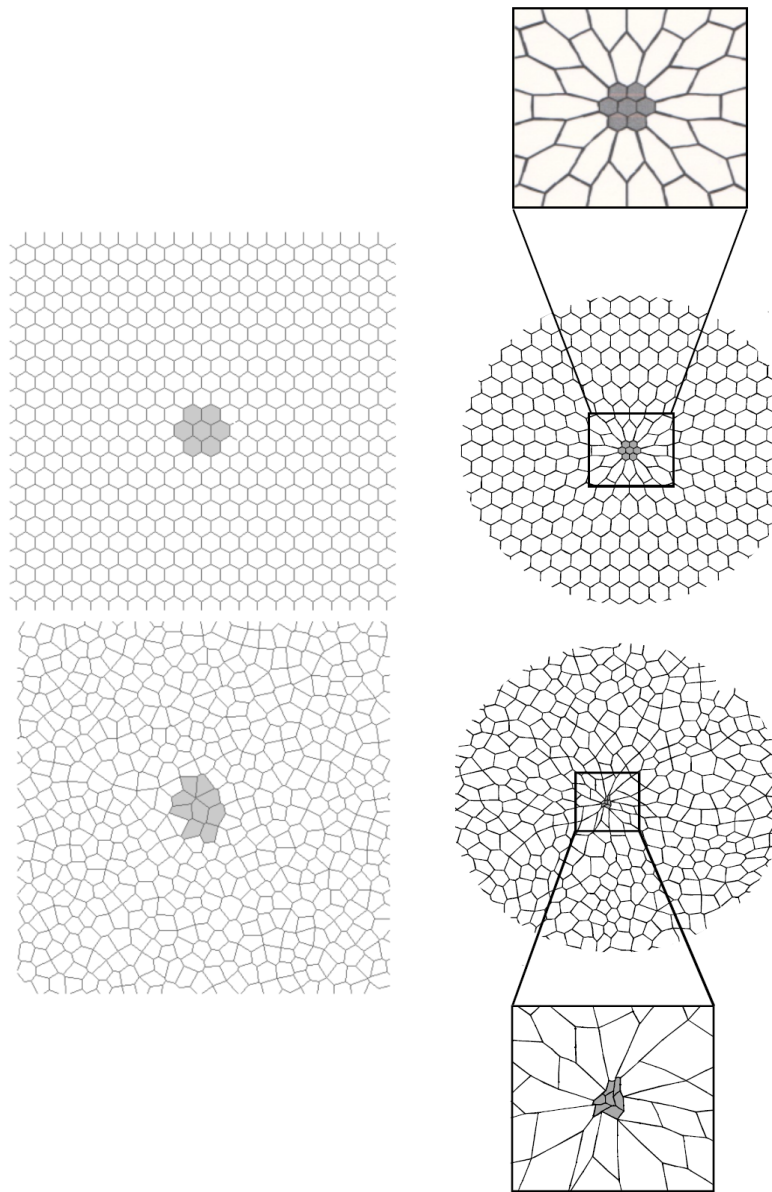
filament, 1 stiff cell, (b) linear elastic filament, 6-9 stiff cells (c) non-linear elastic filament, 1 stiff cell (d) non-linear elastic filament, 6-9 stiff cells. The bold line in each figure is the 2D solution for a rigid cylindrical inclusion in a linear elastic continuum. Strain=15% (◆), strain=30% (■), strain=45% (▲), strain=55% (X).

Figure 7 The radial stress, normalized by the remote stress, plotted against the radial distance from the center of the inclusion, normalized by the inclusion radius, for the 2D and 3D continuum solution for a cylinder and a sphere in a linear elastic medium.

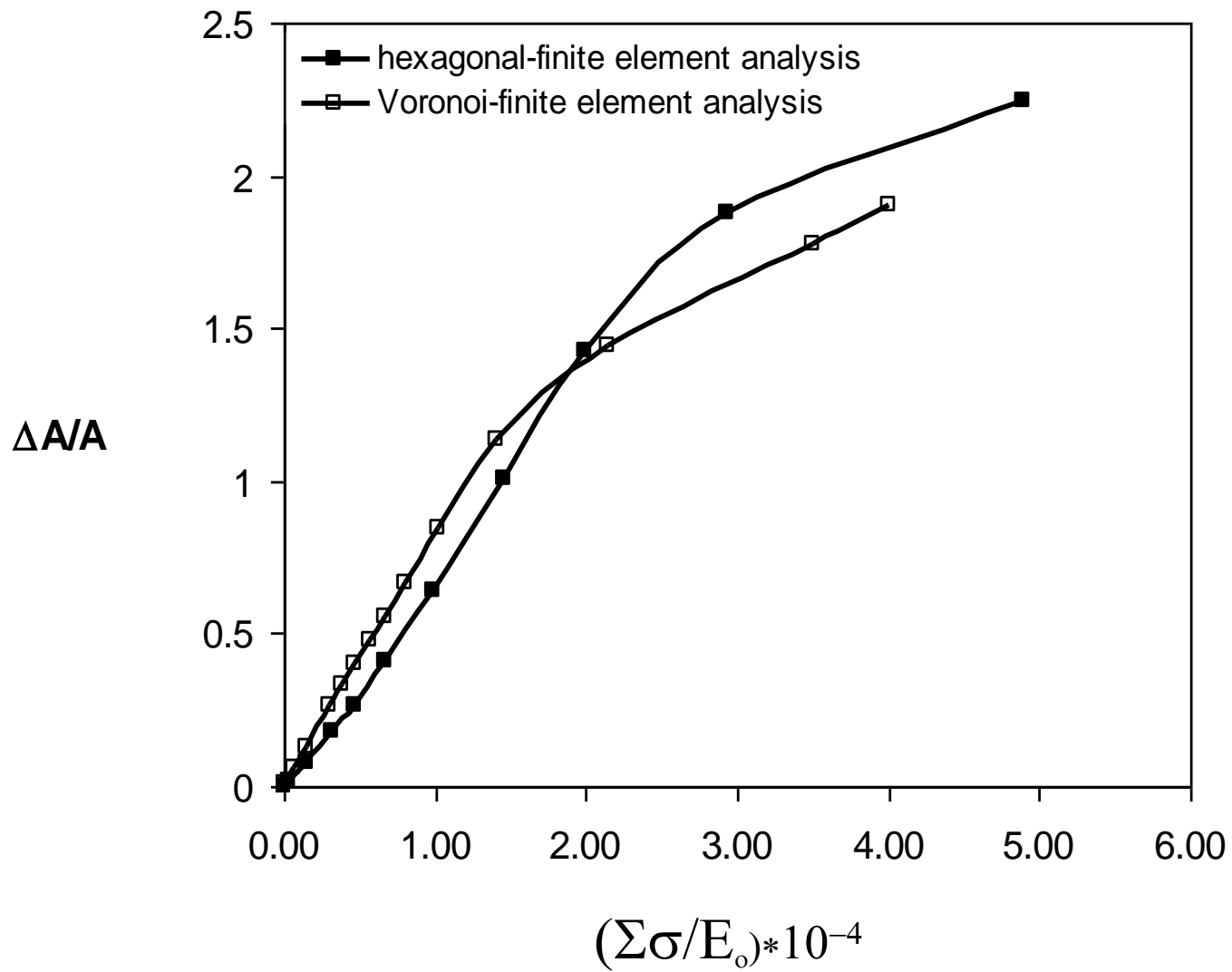


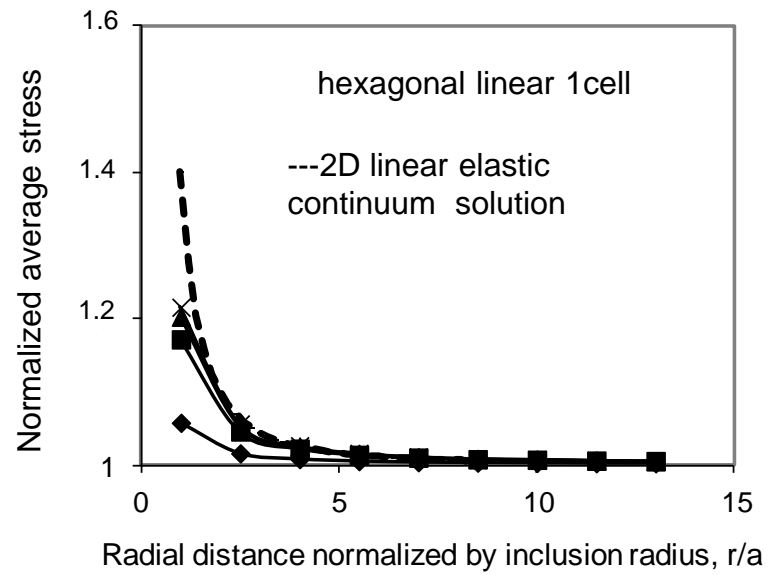


(a)

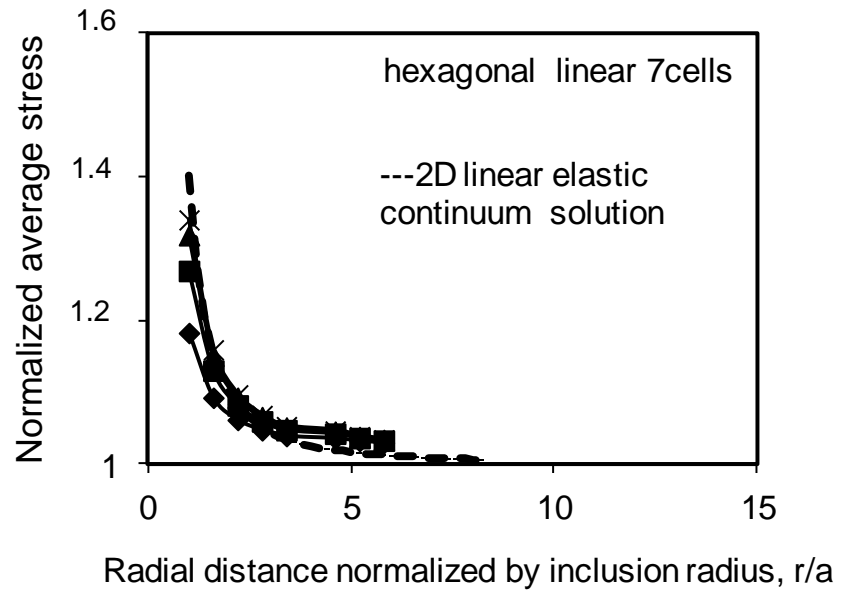


(b)

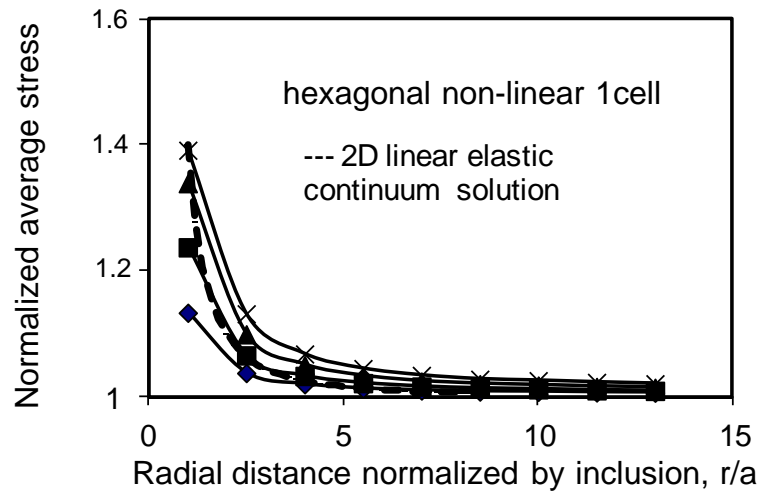




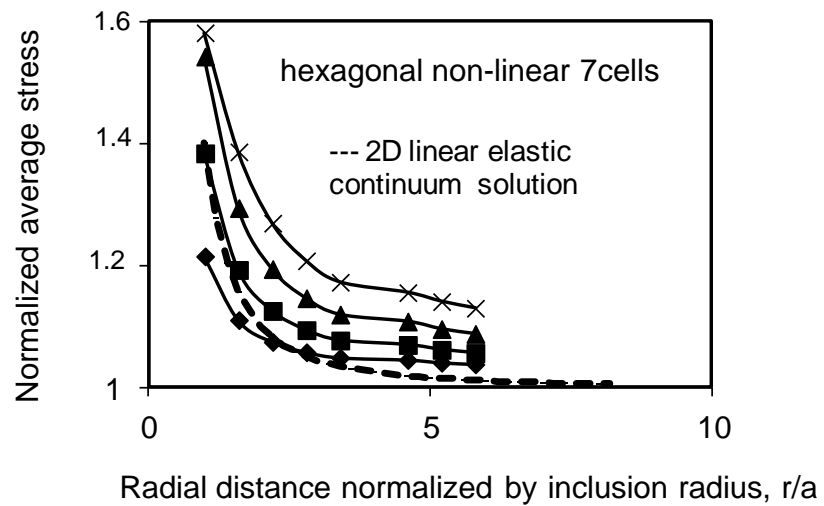
(a)



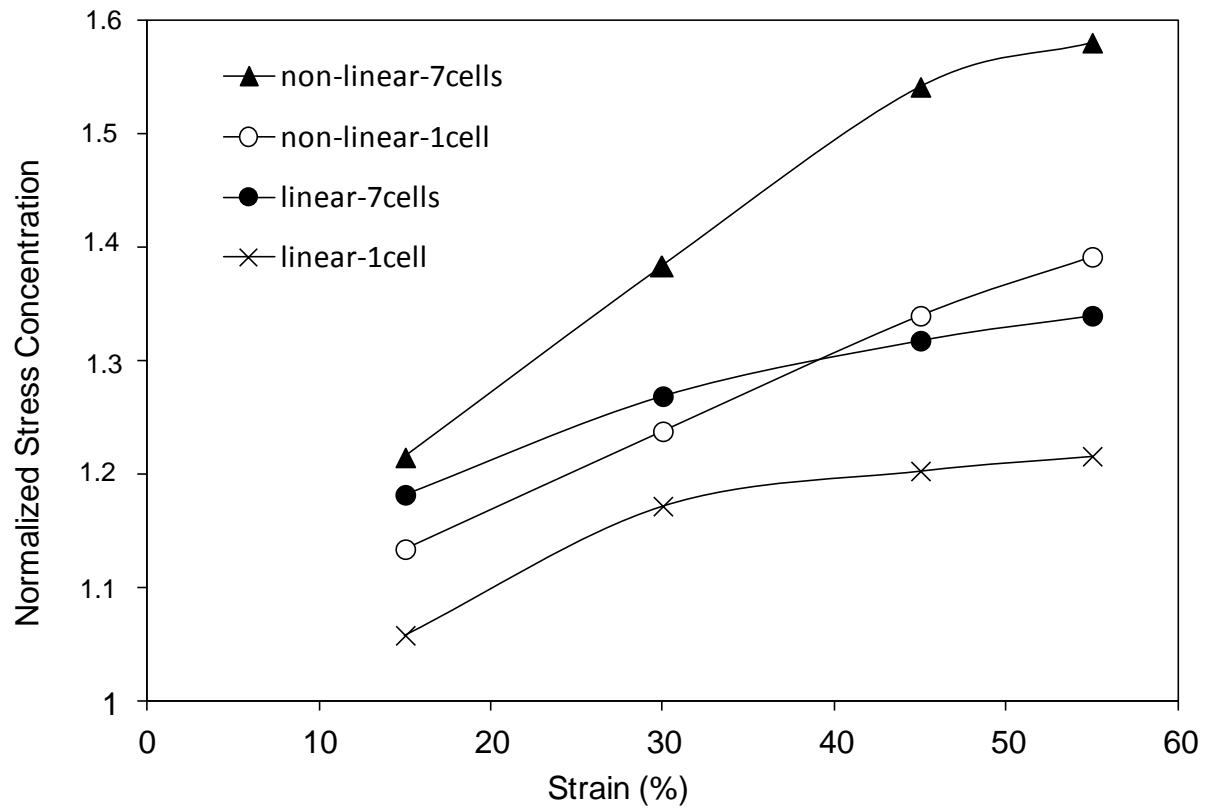
(b)

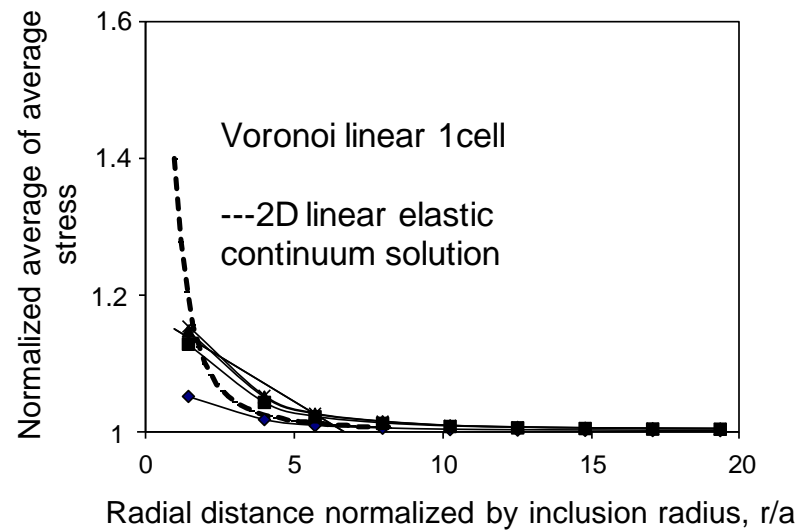


(c)

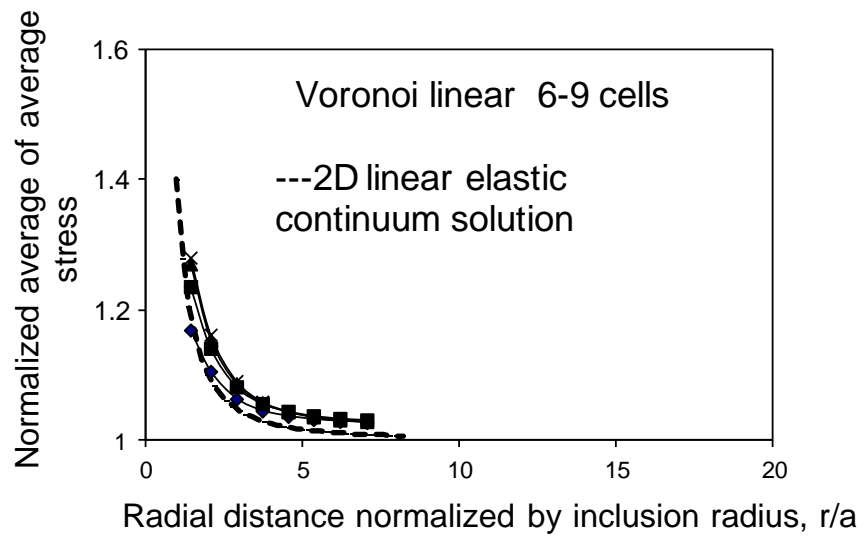


(d)

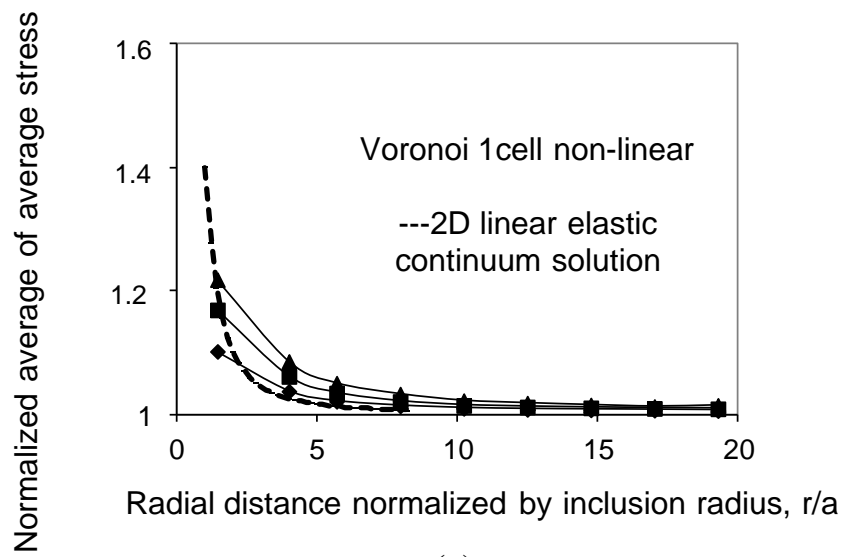




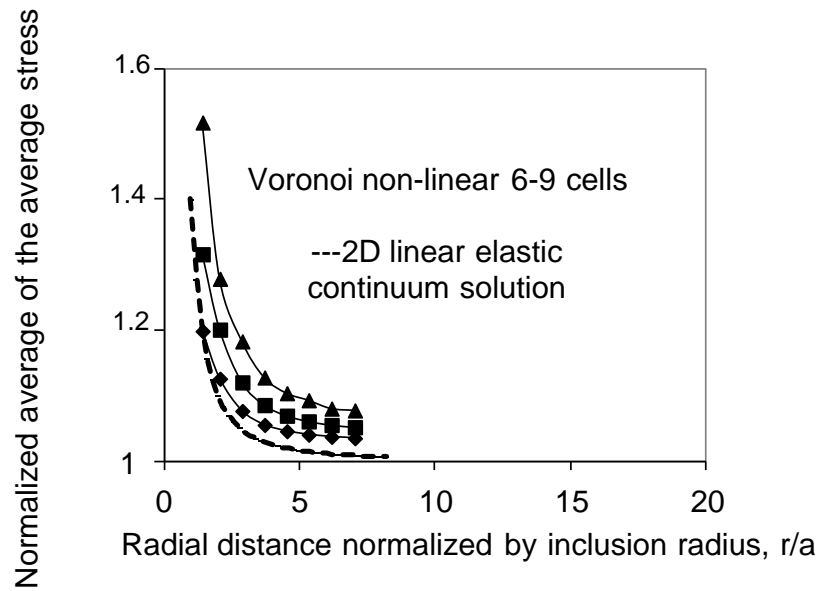
(a)



(b)



(c)



(d)

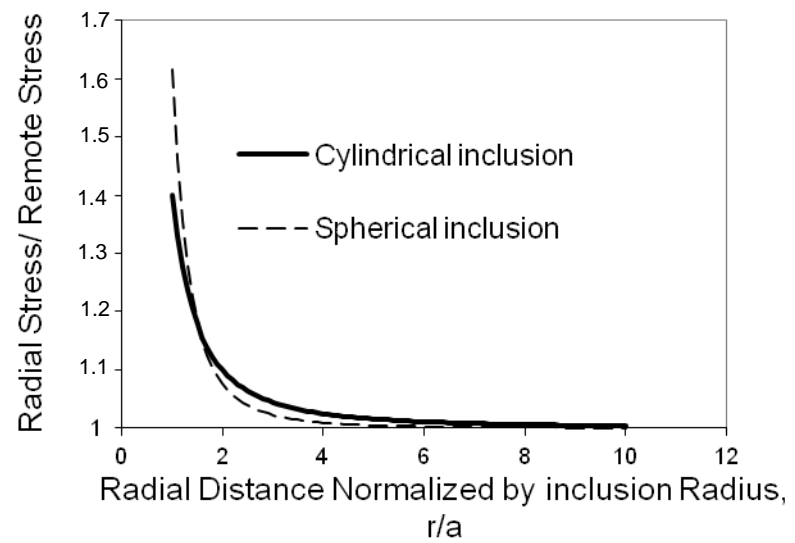


Table 1 Normalized stress in the radial members adjacent to the stiff region in the regular hexagonal honeycombs

Strain	Linear elastic filament 1 cell ^a	Linear elastic filament 7 cells ^b	Non-linear elastic filament, 1 cell	Non-linear elastic filament, 7 cells
15%	1.06	1.18	1.13	1.22
30%	1.17	1.27	1.29	1.38
45%	1.20	1.32	1.34	1.54
55%	1.22	1.34	1.39	1.58

^a 1 cell in the stiff region

^b 7 cells in the stiff region

Table 2 Normalized stress in the radial members adjacent to the stiff region in the Voronoi honeycombs

	Linear elastic filament 1 cell ^a	Linear elastic filament 6-9 cells ^b	Non-linear elastic filament 1 cell (eqn 1)	Non-linear elastic filament 6-9 cells (eqn 1)
STRAIN =15%	-	-	-	-
Average	1.05 (0.024)	1.17 (0.030)	1.10 (0.030)	1.20 (0.029)
avg max	1.09 (0.037)	1.26 (0.043)	1.17 (0.040)	1.30 (0.045)
ind max	1.20	1.37	1.23	1.41
STRAIN=30%	-	-	-	-
Average	1.13 (0.025)	1.24 (0.040)	1.17 (0.030)	1.32 (0.030)
avg max	1.21 (0.023)	1.36 (0.051)	1.27 (0.057)	1.48 (0.059)
ind max	1.25	1.48	1.34	1.63
STRAIN=45%	-	-	-	-
Average	1.15 (0.034)	1.27 (0.044)	1.22 (0.040)	1.52 (0.040)
avg max	1.23 (0.026)	1.41 (0.053)	1.36 (0.078)	2.43 (2.265)
ind max	1.28	1.52	1.46	9.59
STRAIN=55%	-	-		
Average	1.16 (0.037)	1.28 (0.045)		
avg max	1.24 (0.026)	1.43 (0.057)		
ind max	1.30	1.53		

^a 1 cell in the stiff region ^b 6-9 cells in the stiff region

values in brackets are standard deviations

average = the average normalized stress in the radial members in the cells adjacent to the stiff region for all 12 Voronoi honeycombs

avg max = the average, over all 12 Voronoi honeycombs, of the maximum normalized stress in the radial members adjacent to the stiff region in each Voronoi honeycomb

ind max = the individual maximum normalized filament stress of all the filaments in all 12 Voronoi honeycombs (This was always a filament in the radial orientation.)